LAWRENCE
LIVERMORE
NATIONAL
LABORATORY

LLNL-JRNL-649338

GROUND-STATE PROPERTIES OF RARE-EARTH METALS: AN EVALUATION OF DENSITY-FUNCTIONAL THEORY

P. Soderlind, P. E. A. Turchi, A. Landa, V. Lordi

February 6, 2014

Journal of Physics: Condensed Matter

Disclaimer

Ground-state properties of rare-earth metals: An evaluation of density-functional theory

Per Söderlind, P.E.A. Turchi, A. Landa, and V. Lordi
Condensed Matter and Materials Division,
Lawrence Livermore National Laboratory, Livermore, CA 94550, USA

Abstract

The rare-earth metals have important technological applications due to their magnetic properties but are scarce and expensive. Development of high-performance magnetic materials with less rare-earth content is pursued but theoretical modeling is hampered by complexities of the rare earths electronic structure. The existence of correlated (atomic-like) 4*f* electrons in the vicinity of the valence band makes any first-principles theory exceedingly difficult. Nevertheless, we apply and evaluate the efficacy of density-functional theory for the series of lanthanides (rare earths) investigating the influence of the electron exchange and correlation functional, spin-orbit interaction, and orbital polarization. The results are compared with those of the so-called "standard" model of the lanthanides in which electrons are constrained to 4*f* core states with no hybridization with the valence electrons. Our results suggest that spin-orbit coupling and orbital polarization are important, particularly for the magnetic properties, and that calculated equilibrium volumes, bulk moduli, and magnetic moments show correct trends overall. However, the precision of the calculated properties is not at the level of that found for simpler metals in the Periodic Table, and the electronic structures do not accurately reproduce x-ray photoemission spectra.

1. Introduction

The fourteen rare-earth (RE) metals, or lanthanides, belong to a large group in the Periodic Table with most interesting and important properties. They constitute integral components in many technologies including electric motors, alternators, and lasers. The rare-earth metals are special in that they are the first elements with *f* electrons (4*f*) that, in turn, provide for the magnetic properties often utilized in applications. Dominating as they are in this respect, the 4*f* electrons do not significantly influence chemical bonding between the atoms in the solid. Therefore, the *s*, *p*, and *d* electrons in the valence band mostly determine atomic volumes, crystal structures, and strength characteristics. Consequently, these properties vary slowly over the series of lanthanides even though there is a continuous increase in 4*f* electrons from 1 (Ce) to 14 (Lu). The conceptual understanding of this interesting behavior of the 4*f* electrons is that they are localized at their respective atom with very little direct overlap (weak inter-atomic bond) while enough hybridized with the valence band to sustain magnetic order through the crystal at low temperatures [1]. The degree of "localization" or atomic-like character of the 4*f* electrons may change when the RE metal is part of a compound, or being alloyed due to the altered chemical environment. Also, temperature and pressure in particular play roles in the localization process [2].

Because RE metals are scarce and expensive, one seeks to minimize their usage in applications, searching for new materials, without sacrificing magnetic properties and performance. Theoretical modeling of the RE-metal bearing materials is necessary for aiding in this process but made difficult by the aforementioned 4*f*-electron correlation effects (localization). Density-functional theory (DFT) provides a practical framework that can be used to calculate ground-state properties of materials in general but does not in its standard form adequately address strong electron correlation. Alternatively, self-interaction corrected (SIC) DFT, dynamical mean-field theory (DMFT), and DFT plus Hubbard *U* formalism has been applied to specific RE metals, but not to the entire series. To our knowledge, only the "standard" model for lanthanides, within DFT, has been applied for all lanthanides [3, 4].

In this article, our aim is to go beyond the "standard" model (described below) and apply DFT with spin and orbital polarization combined with spin-orbit interaction for

the rare earths. It is critical to evaluate the model for the complete set of metals in the series so that behaviors, if not highly accurate numbers, can be compared to experimental data. Many times the trend of a property can provide important insights and help advance the overall understanding of the materials, and be used as a guideline to select appropriate solutes that minimize the use of RE metals.

Assuming that the degree of 4*f* localization is greatest for the elemental metals themselves, together with their oxides, the DFT model will address a "worst case scenario", and will be expected to improve when applied for materials of more interest for applications such as RE intermetallic compounds and alloys.

In Sect. 2 we state important details of our models and computations for which we present our results with discussions in Sect. 3. Finally, in Sect. 4, we conclude with a general discussion.

2. Computational Details

All calculations are performed within the framework of DFT, and the necessary assumption for the unknown electron exchange and correlation functional is that of the local density approximation (LDA) [5] and generalized gradient approximation (GGA) [6]. Our particular implementation is based on the full-potential linear muffin-tin orbitals (FPLMTO) method that has recently been described in detail [7]. All calculations are spin polarized (SP) with a ferromagnetic configuration either without spin-orbit coupling (SOC), with SOC, and SOC with orbital polarization (OP). The OP has been implemented in the FPLMTO as a parameter-free scheme where an energy term proportional to the orbital moment is added to the total energy functional to account for intra-atomic interactions. The orbital polarization often behaves as a magnification of the SOC with larger orbital moments as a result. The prescription has been utilized and detailed in studies of praseodymium metal [8, 9] in the past.

Most calculations are performed with the 4*f* electrons occupying valence band states and either with SP, SOC, or OP, for both LDA and GGA. We refer to this model below as the "4*f*-band" model. Specifically for this model, we associate a set of semi-core states 5*s* and 5*p* and valence states 6*s*, 6*p*, 5*d*, and 4*f* to two kinetic energy parameters for a so-called double basis set, where SOC and OP are applied only to the *d* and *f* states.

For comparison with previous investigations [3, 4] we also perform calculations within the standard model for lanthanides, the "4*f*-core" model. In this case, as was done in [3, 4], a double-basis set with semi-core 5*p*, valence 6*s*, 5*d*, and 5*f* states, is utilized with the 4*f* electrons occupying core states. Here, neither of SP, SOC, or OP is applied, consistent with [3, 4]. This model thus constrains the 4*f* electrons in the DFT treatment and cannot self-consistently produce a magnetic moment (since the core is not spin polarized).

Because we are fundamentally interested in the trends of properties in the series we only consider the face-centered cubic (fcc) crystal structure in all calculations. However, test calculations for Sm in the hexagonal close-packed (hcp) structure suggest negligible differences in the calculated properties between these two phases. It should be noted that both fcc and hcp are close-packed but with different stacking order of the hexagonal planes (as all RE structures are).

In all present calculations the sampling of k points in the Brillouin zone (BZ) for the appropriate summations are carefully checked for convergence, and 4000 k points are typically used in the irreducible wedge of the BZ. The equilibrium atomic volumes and bulk moduli are obtained from fitting the total energies to a Murnaghan analytic form [10] over a relatively wide volume range of ±10% of the equilibrium volume.

3. Results and discussions

First, we apply the 4*f*-band model for the atomic volumes of the trivalent RE metals in Fig. 1. The divalent Eu and Yb are not considered because in the 4*f*-band model there is no procedure to promote 4*f* electrons at the expense of the *s*, *p*, and *d* valence electrons. The results in Fig. 1 are from calculations that include SOC and OP, which both help to improve the agreement with experimental room-temperature data [11], see Table 1 where all results are listed. Obviously, GGA produces atomic volumes closer to experiments [11] with the notable exception of Sm. However, as the trend in the volumes shows similar positive slope before Sm, while it should actually be weakly negative, we conclude that the LDA has a fortuitous better agreement with experiment in this case. The difficulties the 4*f*-band model has for Sm, and to a lesser extent Tm, see Fig. 1, may be related to inaccuracies in the magnetic properties (see discussion below). Overall, the

GGA results compare rather favorably with handbook data, particularly for the heavier RE metals (Gd to Lu). The LDA accurately reproduces the volume trend of the GGA calculations, but numerically the volumes are too small.

Next, the atomic volumes are calculated within the 4*f*-core model, see Fig. 2. In this scenario it is straightforward to address both the divalent and the trivalent states because the number of 4*f* electrons constricted to the core can easily be changed (one added from the valence electrons for the divalent metal). From Fig. 2 it is clear why the standard (4*f*-core) model for the lanthanides has been used in the past [3, 4]. The GGA duplicates very accurately the experimental volumes from Gd and on. The LDA once again suggests some over-binding with too small volumes throughout. Notice, however, that both GGA and LDA do not accurately predict the experimental trend for the early lanthanides, as was also reported in Refs. [3, 4]. Hence, the standard model appears to break down to some extent for the light RE elements.

The bulk modulus (B) is generally more difficult to calculate accurately even for much simpler materials. For the 3*d* transition metals, for example, the bulk moduli are on average 12% and 26% too large for GGA and LDA, respectively [12]. In Fig. 3 we display the 4*f*-band bulk modulus, again with the full theoretical treatment (OP) together with an average of experiments taken from Ref. [13, 14]. Lesser treatments (SP, and SOC) worsen the comparison with experiments but not dramatically so (not shown). Surprisingly, Fig. 3 indicates that the LDA bulk moduli are generally better than those obtained within the GGA. However, the reason for this is simply cancellation of errors within the LDA because the LDA volumes (Fig. 1) are so small that the bulk moduli become artificially large. This fact is highlighted in Fig. 3 where the LDA bulk moduli, evaluated at the experimental equilibrium volume (V_0), are displayed. Clearly, these are in substantially worse agreement with experiment than the GGA results. Evaluating B at V_0 does not change the GGA results significantly because the GGA equilibrium volumes are much closer to V_0.

We also calculate B for the 4*f*-core model (not shown) and got very similar results to that of Delin *et al.* [3, 4]. Relative to the 4*f*-band model, these bulk moduli are generally larger, and much too large for the early RE metals.

Even though SOC and OP improve the bonding properties throughout the lanthanide series, these interactions have a more significant impact on the magnetic properties. In Fig. 4 we contrast the calculated total magnetic moments (spin and orbital contributions) with tabulated data [15]. In the upper panel (a) the SP results show a continuous increase of the total (spin only) magnetic moment up until Gd, where a maximum is reached. This is reminiscent of the behavior of the spin moment in the magnetic 3*d* transition metals (Fe-Ni) that follows the so-called Slater-Pauling curve. The spin moment increases until the band is half full (one spin band is completely full), then it decreases as the other spin band is gradually occupied. For *d*-transition metals the spin maximum occurs for 5 *d* electrons (out of a total of 10 *d* electrons), but here it occurs for 7 *f* electrons (Gd) because the *f* band can host 14 electrons. Unfortunately, the SP model is completely incapable of reproducing the experimental trend of the total magnetic moments.

Including spin-orbit coupling is particularly important for the magnetic properties because it gives rise to an orbital magnetic component that is sizeable in most RE metals. In Fig. 4 (b) the total (spin and orbital) magnetic moments from the SOC calculations are shown and, compared to those based on SP computations, they are smaller for the lighter, and greater for the heavier metals, improving the comparison to experimental data. The reason is that for less than half-filled 4*f* shell the orbital moment aligns anti-parallel with the spin moment, reducing the total moment, while the opposite occurs for more than half filled 4*f* shell. In spite of this, there is still a significant discrepancy with experimental magnetic moments for the SOC calculations.

Advancing the theory to include OP is much improving the magnetic moments in the RE metals as can be seen in Fig. 4 (c). In this case both the overall trend and the actual magnitudes are very reasonable considering the electron localization problem discussed earlier. Nonetheless, the results for Sm and Tm overestimate and underestimate the total magnetic moment, respectively. Interestingly, the model underperforms for these two metals in terms of the atomic volume as well (Fig. 1). Both Sm and Tm precede the divalent metals Eu and Yb that have half and fully filled 4*f* shell, respectively. For the half and full shell configurations the orbital moment completely cancel, and perhaps the

closeness to these stable configurations for Sm and Tm results in too small orbital moments.

Let us next consider the calculated orbital magnetic moments (GGA and OP) displayed in Fig. 5. Here our suspicion is confirmed: the orbital moments for both Sm and Tm are significantly smaller in magnitude than a continuous interpolation between the other RE metals suggests. In this figure we associate all orbital moments, except those of Sm and Tm, to a cubic spline that shows a smooth behavior with Sm and Tm being outliers. The underestimation of the orbital moments for Sm and Tm suggests that the 4*f* band has more occupation than it should (too much anti-bonding), resulting in a loss of chemical bonding. Obviously, this also explains, as a result, why the model overestimates the atomic volumes for Sm and Tm, as shown in Fig. 1.

From Fig. 4 we can conclude that both SOC and OP are very important for the correct trend but only with reasonable OP magnitudes of the moments are achieved. The influence of the electron exchange and correlation approximation (LDA or GGA) is much less pronounced but it is more significant for calculated atomic volumes and bulk moduli, as discussed earlier.

The calculated (4*f*-band) electronic spectra do not agree well with photoemission measurements for the RE metals because the 4*f* band orbitals are too broad (delocalized) to properly account for the limited spatial extent of the localized 4*f* states, and too large in energy as well. We illustrate this observation in Fig. 6 for praseodymium where the measured x-ray photoemission spectrum [16] is compared to the calculated electronic density of states convoluted with lifetime and instrumental broadening. Notice that, in particular, the final state, $^2F_{5/2}$, is not at all reproduced in 4*f*-band model that instead predicts large weight of 4*f* states close to the Fermi level (with the highest occupied energy taken as zero of energy).

4. Summary and conclusion

We performed DFT calculations for the RE metal series to investigate primarily ground-state equilibrium volumes, bulk moduli, and magnetic moments. The principal theoretical treatment includes spin polarization, spin-orbit coupling, and orbital

polarization for the 4*f*-band model. For comparison with previous works we also consider the standard model for lanthanides (4*f*-core).

It is satisfying to note that the most advanced theory (GGA+OP) produces the best results overall, and that equilibrium volumes, bulk moduli, and magnetism can all be reasonably well described within one parameter-free model. Certainly, there are approaches for strongly correlated electrons, including "SIC-DFT" [17], "LDA+U" [18], "DMFT" [19], and Hubbard model [20] that reproduce some aspects better for specific RE metals. These models, however, tend to depend on adjustable parameters in some form, and therefore generality and predictability can be questioned. The DFT, on the other hand, can be utilized with no adjustment, and this makes the methodology appealing to use in the search for new materials or for conditions where experiments have not been carried out.

The degree of 4*f*-electron localization, for example, is expected to change with pressure when 4*f*-orbitals near each other begin to overlap. This electron "delocalization" is believed to be responsible for volume collapses and associated phase transitions to more complex crystal structures. Models that are constrained, either by parameters or by its construct, to represent the localized 4*f*-electron behavior may not be able to foresee such pressure-induced phenomena. To illustrate this we show in Fig. 7 calculated total energies for Pr as functions of volume for the 4*f*-band and 4*f*-core models. First we realize that the energy increase is much larger with compression for the latter model, giving rise to an unrealistically "stiff" equation of state. In addition, only the 4*f*-band model is able to reproduce the known phase transition to the orthorhombic α-U phase. In contrast to the 4*f*-core model, the pressure behavior of Pr reproduces the experimental data rather well for the 4*f*-band model [9].

Despite the limitations clearly revealed in this study, parameter-free electronic structure calculations founded on DFT can be useful for identifying trends in solute effects on stability and magnetic properties in RE-based multi-component alloys, and this knowledge can provide useful guidance for selecting specific solutes that minimize the usage of RE metals without altering materials performance.

Acknowledgements

This work performed under the auspices of the U.S. DOE by LLNL under Contract DE-AC52-07NA27344. This research is supported by the Critical Materials Institute, an Energy Innovation Hub funded by the U.S. Department of Energy, Office of Energy Efficiency and Renewable Energy, Advanced Manufacturing Office.

References

1. B. Johansson and M. S. S. Brooks, in *Handbook on the Physics and Chemistry of the Rare Earths*, edited by K. A. Gschneidner Jr., L. Eyring, G. H. Lander, and G. R. Choppin (North-Holland, Amsterdam, 1993), Vol. 17, Chap. 112, p. 149.
2. B. Johansson, H. L. Skriver, and O. K. Andersen, in *Physics of Solids under High Pressure*, edited by J. S. Schilling and R. N. Shelton (North-Holland, Amsterdam, 1982), p. 245.
3. A. Delin, L. Fast, O. Eriksson, and B. Johansson, J. Alloys Compd. **275**, 472 (1998).
4. A. Delin, L. Fast, B. Johansson, O. Eriksson, and J. M. Wills, Phys. Rev. B **58**, 4345 (1998).
5. U. von Barth and L. Hedin, J. Phys. C: Solid Phys. **5**, 1629 (1972).
6. J. Perdew, J. A. Chevary, S. H. Vosko, K. A. Jackson, M. R. Pederson, and D. J. Singh, Phys. Rev. B **46**, 6671 (1992).
7. J. M. Wills, O. Eriksson, M. Alouani, and D. L. Price, in *Electronic Structure and Physical Properties of Solids*, edited by H. Dreysse (Springer-Verlag, Berlin, 1998), p. 148.
8. A. Svane, J. Trygg, B. Johansson, and O. Eriksson, Phys. Rev. B **56**, 7143 (1997).
9. P. Söderlind, Phys. Rev. B **65**, 115105 (2002).
10. F.D. Murnaghan, Proc. Natl. Acad. Sci. USA **30**, 244 (1944).
11. K. A. Gschneidner Jr., Bulletin of Alloy Phase Diagrams **11**, 216 (1990).
12. V. Ozolins and M. Körling, Phys. Rev. B **48**, 18304 (1993).
13. W. A. Grosshans and W. B. Holzapfel, Phys. Rev. B **45**, 5171 (1992).
14. M. J. Lipp, Y. kono, Zs Jenei, H. Cynn, C. Aracne-Ruddle, C. Park, C. Kenney-Benson, and W. J. Evans, J.Phys.: Condens. Matter **25**, 345401 (2013).

15. K. A. McEwen, in *Handbook on the Physics and Chemistry of Rare Earths*, edited by K. A. Gschneidner and L. R. Eyring (North-Holland, Amsterdam, 1978) Vol. 1, p. 411.
16. J. K. Lang, Y. Baer, and P. A. Cox, J. Phys. F: Metal Phys. **11**, 121 (1981).
17. A. Svane, W. M. Temmerman, Z. Szotek, J. Laegsgaard, and H. Winter, Int. J. of Quantum Chem. **77**, 799 (2000).
18. B. Amadon, F. Jollet, and M. Torrent, Phys. Rev. B **77**, 155104 (2008).
19. A. K. McMahan, R. T. Scalettar, and M. Jarrell, Phys. Rev. B **80**, 235105 (2009).
20. S. Lebegue, A. Svane, M. I. Katsnelson, A. I. Lichtenstein, and O. Eriksson, Phys. Rev. B **74**, 045114 (2006).

Figure Captions

1. (Color online) Experimental room-temperature atomic volumes [11] with LDA+OP and GGA+OP results (4*f*-band model, see main text). The experimental volume for both α-Ce and γ-Ce is shown.
2. (Color online) Experimental room-temperature atomic volumes [11] with LDA and GGA results (4*f*-core model, see main text). The experimental volume for γ-Ce is shown.
3. (Color online) Experimental average bulk modulus compiled from [13] together with LDA+OP and GGA+OP (4*f*-band model) results. Open symbols refer to LDA+OP calculations of B evaluated at the experimental atomic volume (V_0). For Ce, the experimental result for the α phase (at 1 GPa) is shown [14].
4. (Color online) Experimental total magnetic moments [15] together with results from the 4*f*-band model with SP (a), SOC (b), and OP (c) interactions (see main text).
5. Calculated (GGA+OP) orbital magnetic moments. The solid line is a cubic spline fitted to all moments, except that of Sm and Tm.
6. X-ray photoemission (solid squares) [16] and GGA+OP (4*f*-band model) electronic density of states (with lifetime and instrumental broadening) for praseodymium metal.

7. (Color online) Total energies as functions of atomic volume obtained from the 4*f*-band (dashed) [9] and 4*f*-core model (GGA) for praseodymium metal. Transition to the α-U phase, orthorhombic (Cmcm), is only predicted by the 4*f*-band theory.

Table Caption

1. Experimental room-temperature atomic volumes [11] with the volume for α-Ce given in parenthesis together with theoretical data from various levels of approximation (see main text). All volumes are in units of $Å^3$.

Table 1.

Element	Expt.	LDA-SP	LDA-SO	LDA-OP	GGA-SP	GGA-SO	GGA-OP
Ce	34.3 (28.1)	23.2	23.3	23.3	26.3	26.4	26.4
Pr	34.55	21.1	21.3	26.7	28.3	28.7	33.6
Nd	34.17	23.3	24.1	28.9	34.0	34.0	34.9
Pm	33.6	27.3	28.2	29.8	36.8	36.8	36.0
Sm	33.21	32.1	32.3	32.65	38.1	38.2	38.3
Eu	48.1	–	–	–	–	–	–
Gd	33.1	28.6	28.6	28.6	32.2	31.9	32.0
Tb	31.95	25.6	26.3	27.5	31.3	31.2	32.0
Dy	31.54	26.9	26.9	28.2	33.3	33.2	32.6
Ho	31.11	28.5	27.5	27.5	33.3	33.0	31.7
Er	30.63	26.7	27.7	27.2	31.4	31.2	31.2
Tm	30.16	28.3	28.4	28.4	30.3	30.8	32.4
Yb	41.95	–	–	–	–	–	–
Lu	29.45	25.5	25.4	25.4	28.5	28.4	28.4

Figures

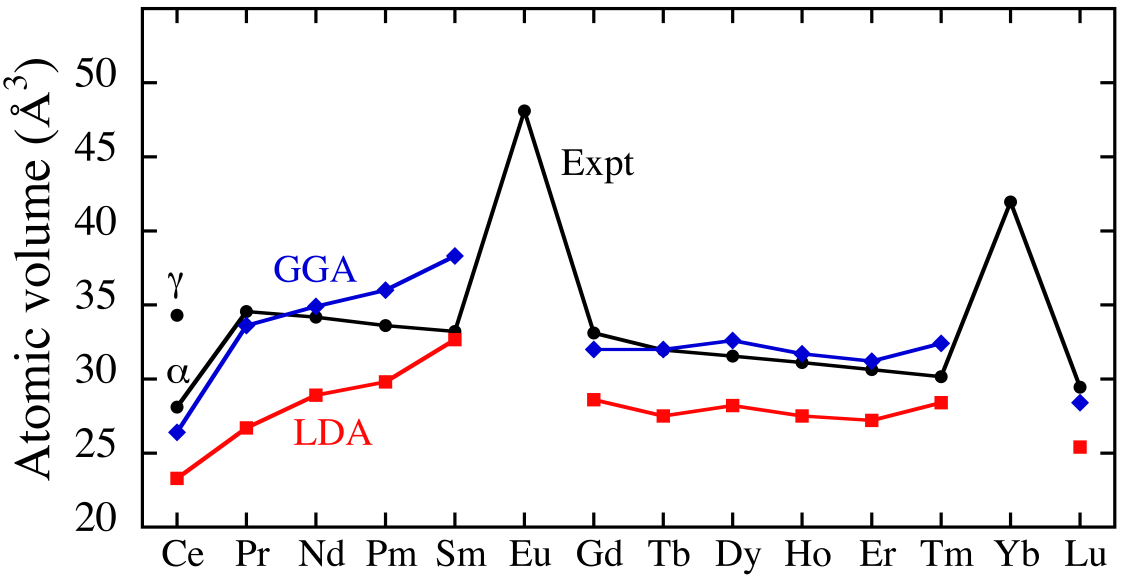

Figure 1.

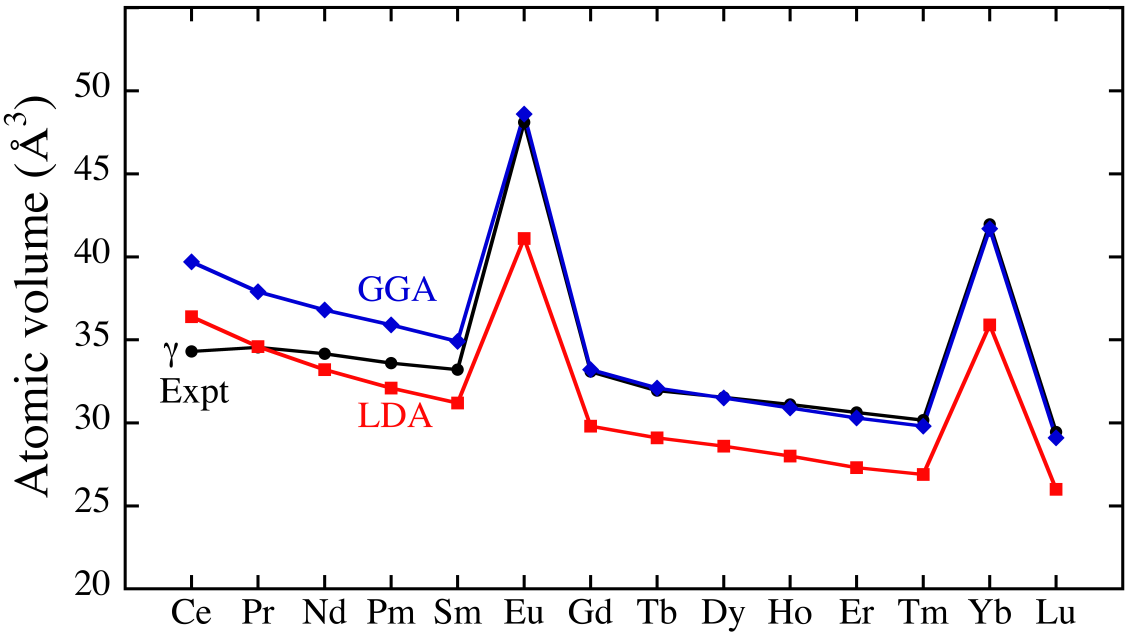
Atomic volume (Å^3)
50
45
40
35
30
25
20
GGA
γ
Expt
LDA
Ce
Pr
Nd
Pm
Sm
Eu
Gd
Tb
Dy
Ho
Er
Tm
Yb
Lu

Figure 2.

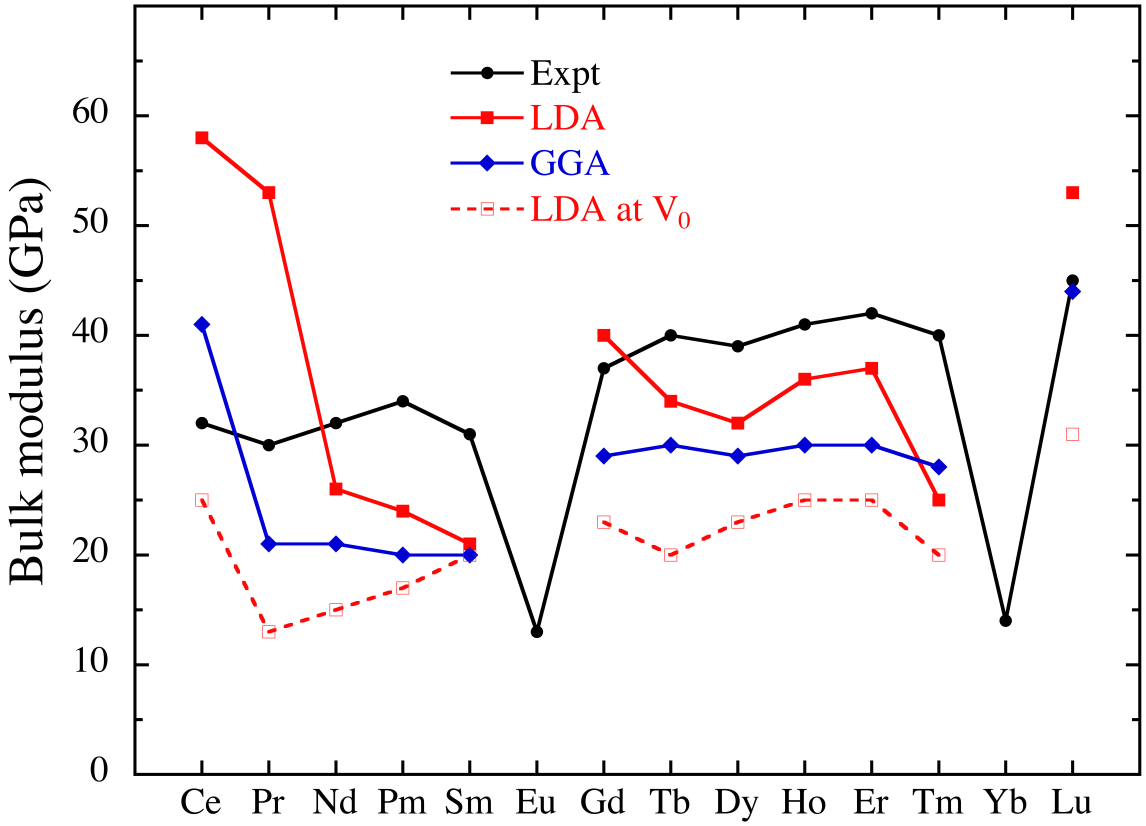
Expt
LDA
GGA
LDA at V0
Bulk modulus (GPa)
0
10
20
30
40
50
60
Ce
Pr
Nd
Pm
Sm
Eu
Gd
Tb
Dy
Ho
Er
Tm
Yb
Lu

Figure 3.

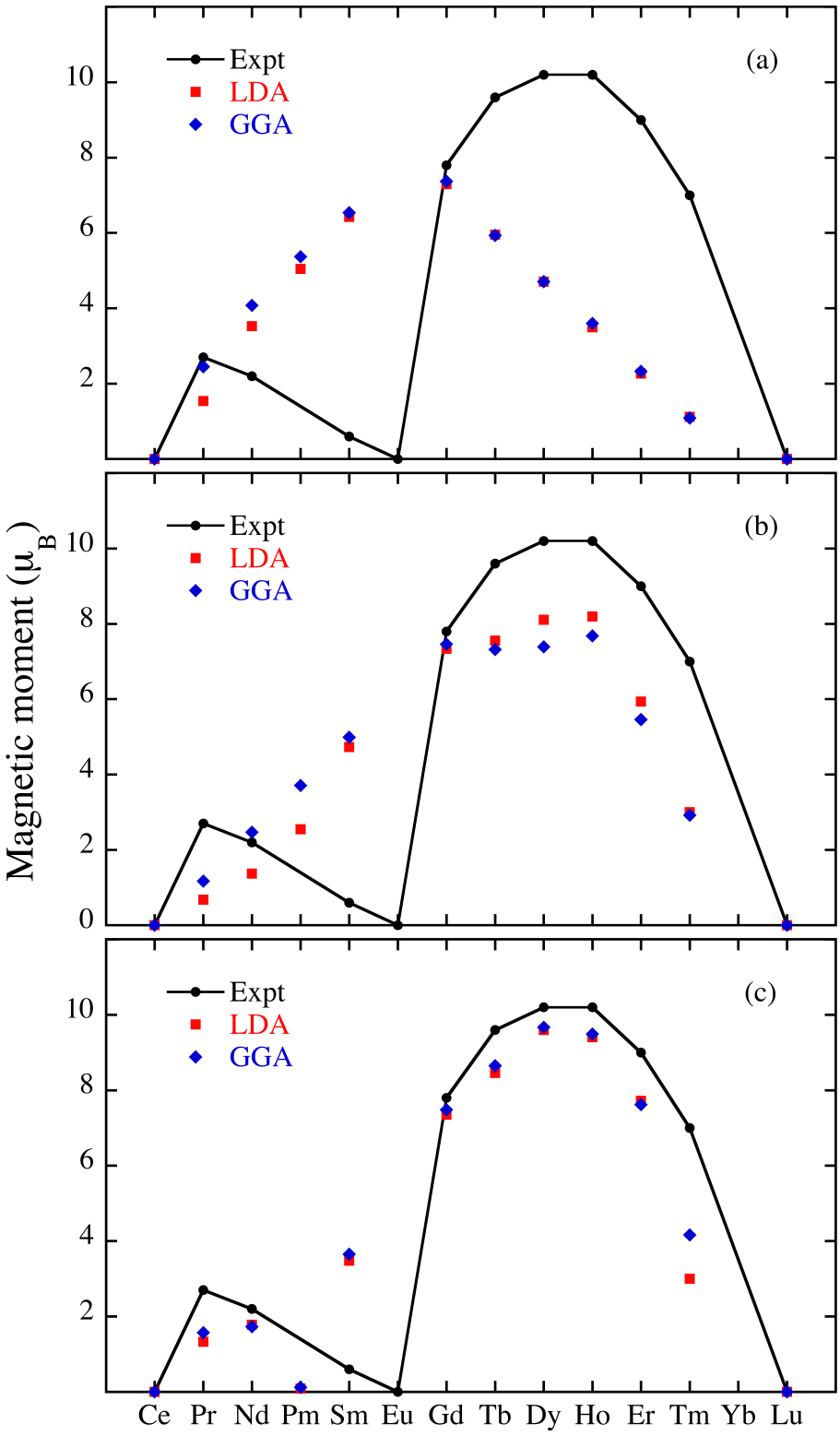
Expt
LDA
GGA
(a)
(b)
(c)
Magnetic moment (μ_B)
0
2
4
6
8
10
Ce Pr Nd Pm Sm Eu Gd Tb Dy Ho Er Tm Yb Lu

Figure 4.

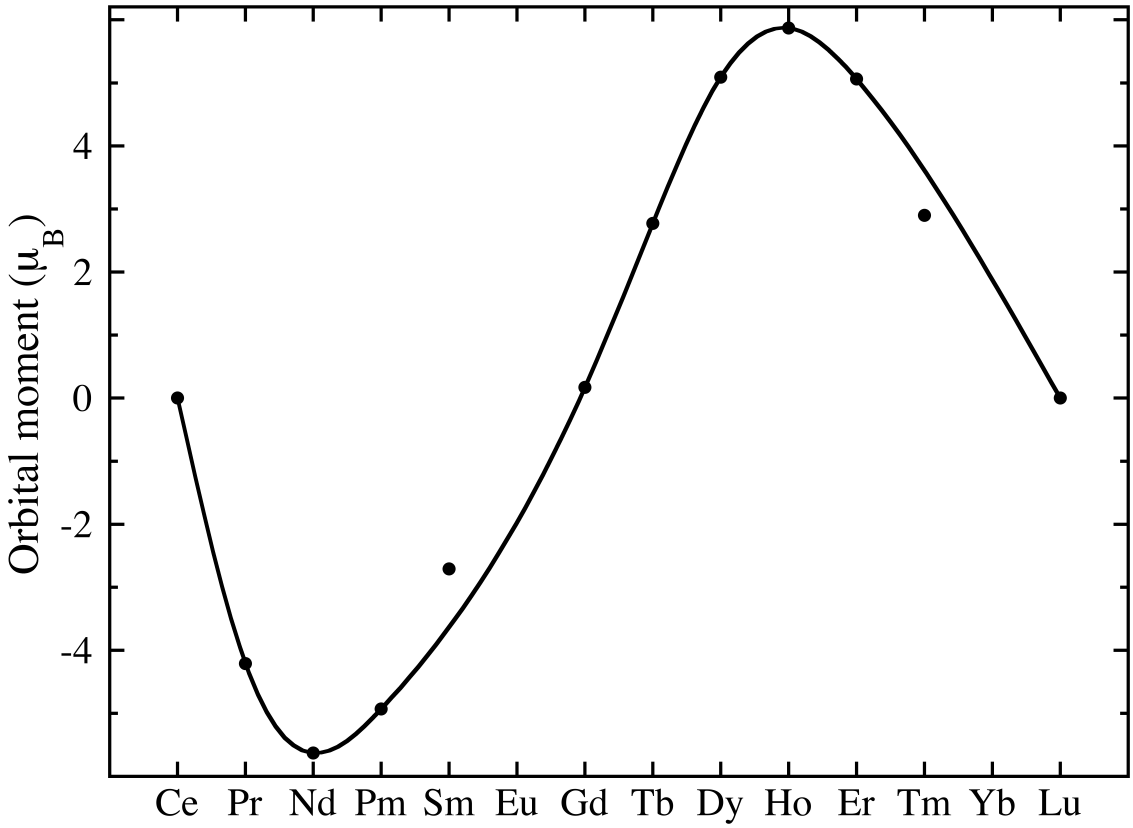

Figure 5.

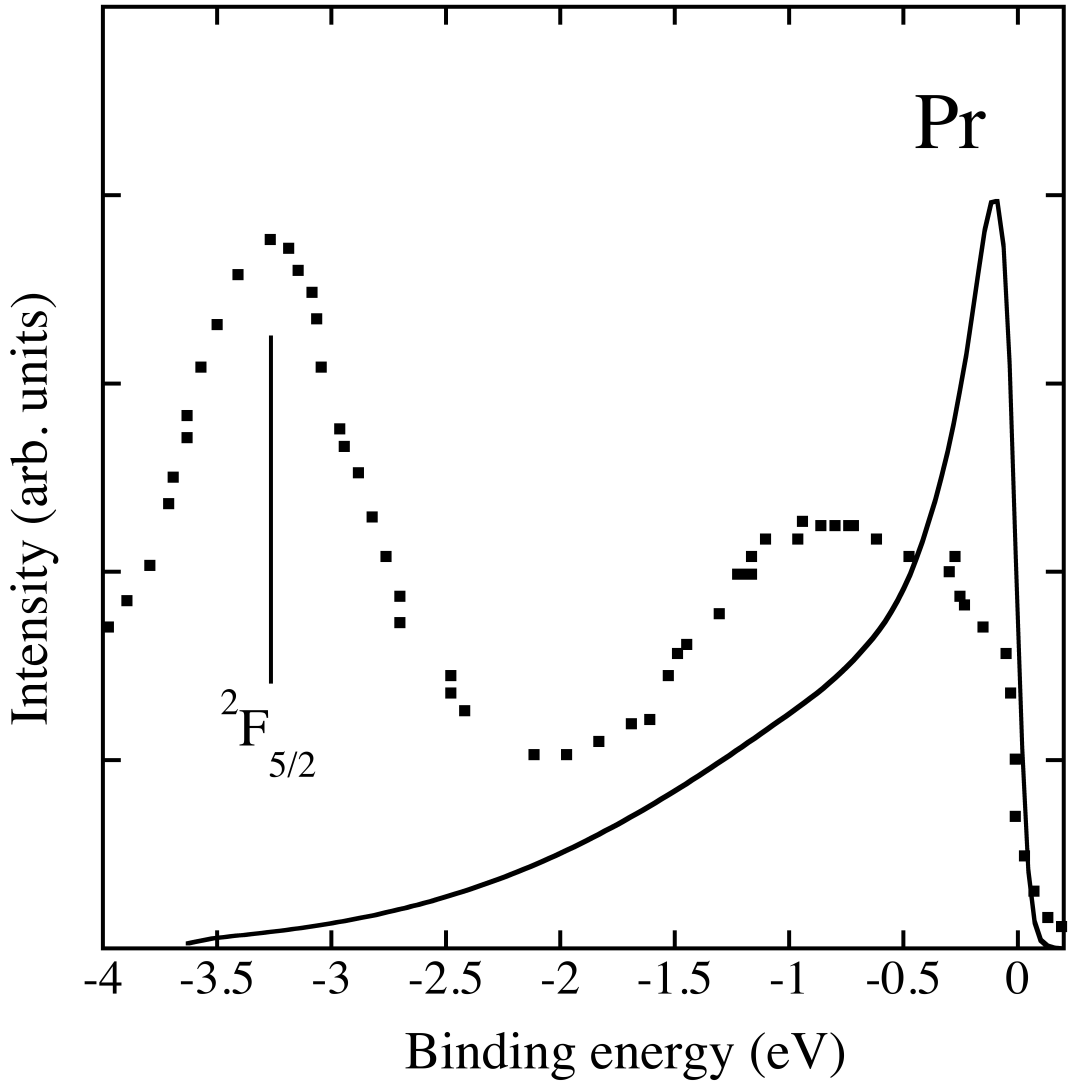
Pr
Intensity (arb. units)
$^2F_{5/2}$
-4
-3.5
-3
-2.5
-2
-1.5
-1
-0.5
0
Binding energy (eV)

Figure 6.

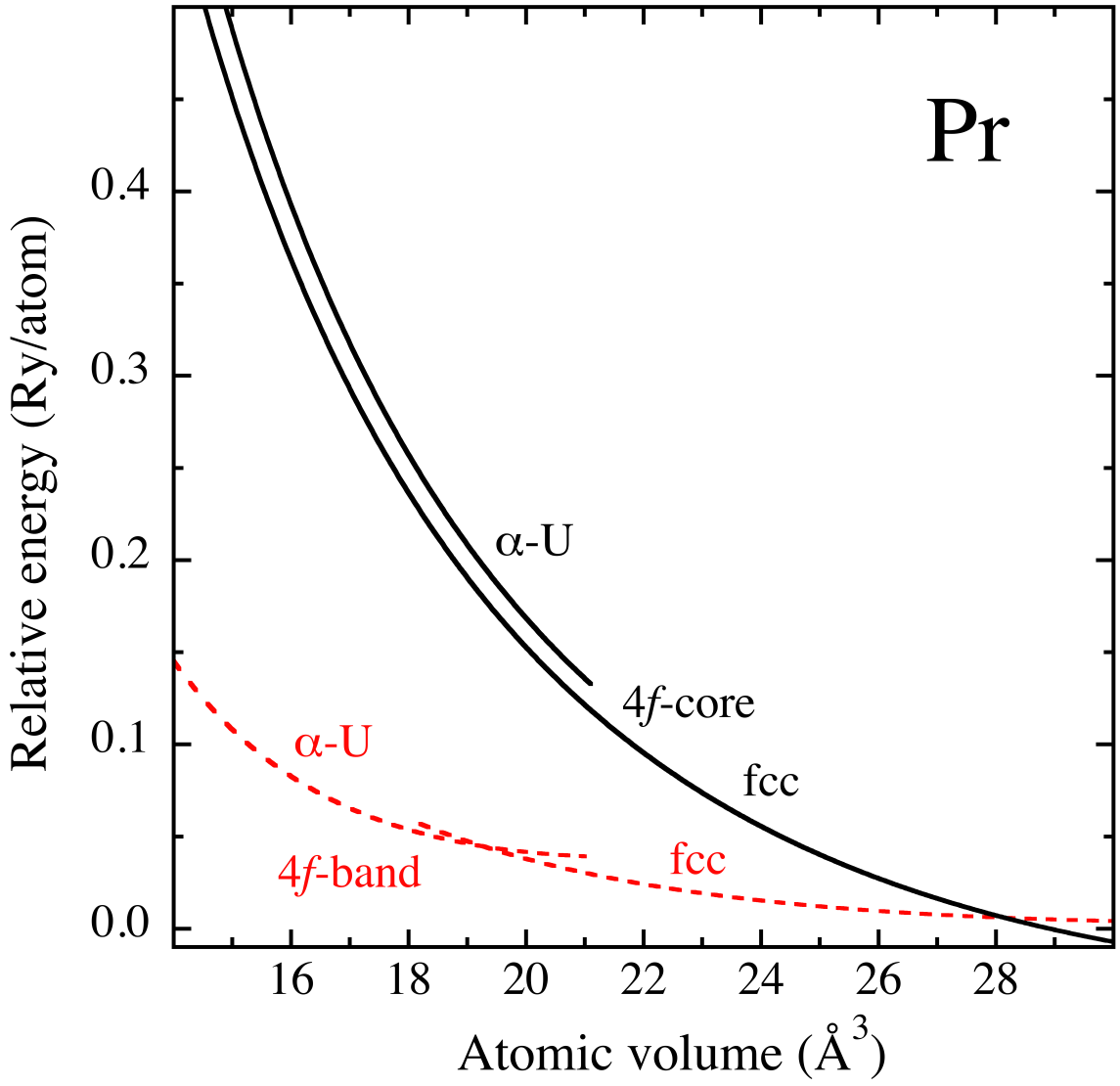
Pr
Relative energy (Ry/atom)
0.0
0.1
0.2
0.3
0.4
16
18
20
22
24
26
28
Atomic volume (Å^3)
α-U
4*f*-core
fcc
α-U
4*f*-band
fcc

Figure 7.